Effects of leading-edge blowing control and reduced frequency on Aerofoil aerodynamic performances

Yang Chen[1], Eldad Avital[1*], John Willams[1], Srimanta Santra[2], Avraham Seifert[3]

1. School of Engineering and Materials Science, Queen Mary University of London, London E14NS, UK
2. Department of Chemical Engineering, Massachusetts Institute of Technology, Cambridge, MA 02139, USA
3. 3.School of Mechanical Engineering, Tel Avia University, 39040, Tel Avia, Israel

*. The Corresponding Author

Abstract

Aerofoil leading edge fluid-blowing control is simulated to improve aerodynamic efficiency. The fluid injection momentum coefficient Cu defined as a ratio between the squares of the injection and incoming velocities times the ratio of the slot's width to the aerofoil's half chord-length varies from 0.5% to 5.4%. Both static and dynamic conditions are investigated for the NACA0018 aerofoil at low speed and Reynolds number of 250k as based on the aerofoil's chord length. The oscillation is achieved by pitching the incoming freestream velocity in a reduced frequency defined as the ratio between the pitching tangential speed (based on half chord-length) to the free stream speed, and which varies from 0.0078 to 0.2.

RANS and Unsteady RANS (URANS) are used in the simulations as based on the Transition SST and Spalart-Allmaras models, generally achieving good agreement with experimental results in lift and drag coefficients, and in the pressure coefficient distributions along the aerofoil. It is found that oscillating the aerofoil can delay stall as expected in dynamic stall. Leading-edge blowing control can also significantly delay stall both in static and dynamic conditions as long as sufficient momentum is applied to the control. On the other hand, for a small Cu as 0.5%, the leading-edge control worsens the performance and hastens the appearance of stall in both static and dynamic conditions. The aerofoil's oscillation reduces the differences between pitch-up and pitch-down aerodynamic performances. Detailed analysis of vorticity, pressure, velocity and streamline contours are given to provide plausible explanations and insight to the flow.

Keywords

Leading-edge fluid-blowing control, Static and oscillating NACA0018 aerofoil, URANS, Stall delay.

1. Introduction

In recent years, the world is grappling with an energy crisis as dwindling fossil fuel reserves and increasing demand put a strain on global energy supplies. The abundance of wind energy has made it one of the pillars of renewable energy strategy worldwide. It is one of the fast-growing industry of renewables, according to BP (BP Public Limited) estimates in 2020, wind power capacity expanded by 111GW- almost double its previous highest annual increase.

Wind turbines have gained popularity worldwide, while seeing technology advances and increased public support for renewable energy. For lift-based wind turbines, one of the main impediments for achieving high aerodynamic efficiency (lift to drag ratio) is the occurrence of dynamic stall (DS)[1]. It can also result in a dynamic blade loading and fluctuating energy harvesting. Horizontal axis wind turbines (HAWT) can encounter DS due to surrounding conditions of strong turbulence in the incoming wind while trying to achieve high angle of attack (AoA) to yield high lift [2]. However, the vertical axis wind turbine (VAWT) by its nature is prone to dynamic stall at low to mid tip speed ratios (TSRs). It is caused by the alternating direction of the blade as relative to the wind direction during the cycle of rotation, while the blade encounters high AoAs during that cycle [3] . The occurrence of DS in a blade typical to VAWT and DS mitigation using active flow control at the leading edge of the blade is the topic of this research.

According to Leishman[4], dynamic stall is a complex aerodynamic phenomenon occurring when there is a rapid change in the angle of attack of an aerofoil, such as plunging or vertical translation, or other types of motion that take the effective angle of attack above its normal steady stall angle. During dynamic stall, the boundary layer on the upper surface of the aerofoil separates and reattaches in a highly unsteady and turbulent manner, resulting in complex flow structures and vortices that can interact with the blade, which differ fundamentally from the stall mechanisms observed for the same aerofoil under static (quasi-steady) conditions[5].

Stated simply, the initiation of dynamic stall can be described as the creation of a leading-edge vortex (LEV) that separates from the aerofoil's surface and is carried along the upper side, leading to a sudden increase in lift and drag forces. As the angle of attack further increases, the LEV expands in both size and intensity until it eventually collapses, leading to a sudden drop in lift and a sharp increase in drag [5][6] . This behaviour can produce hysteresis loops in the force coefficients, producing cyclic pressure loadings.

Various control techniques have been used to mitigate dynamic stall in aerofoils. The control strategies relevant within the scope of this study can be grouped into two main categories, namely, the active and passive flow control approaches. Passive flow control methods, including vortex generators, Gurney flaps, micro tabs, and leading-edge slats, are commonly utilized and require no external power source. On the other hand, active flow control techniques, such as leading-edge slot blowing [7][8][9] , oscillating flaps[10] , dielectric barrier discharge plasma actuators [11][12], and synthetic jets[13], have also been extensively investigated. Hence, active flow control methods may have the capability to delay or even eliminate dynamic stall by manipulating the control parameters.

As the dynamic-stall vortex develops close to the aerofoil's leading edge, dynamic-stall-control devices are assumed to be most efficient if they are located close to or at the leading edge to influence the dynamic-stall vortex at its origin [14][15]. The present investigation motivates the use of leading-edge slot blowing as a relatively simple mean of a dynamic stall control. In 1904, Prandtl's formulation of boundary-layer theory marked a significant milestone in boundary-layer control (BLC) research[14]. Slot blowing, alongside constant suction, was among the earliest control concepts explored. Since the early 1920s, researchers have studied the effects of steady blowing from control slots positioned on the suction surface of aerofoils, leading to notable improvements in lift generation [15][16][17] . When the momentum of the jet exceeds a critical value, the boundary layer becomes more resistant to separation. This demonstrates the traditional application of constant blowing, where the surplus momentum near the wall counteracts the adverse pressure gradient that would otherwise induce separation (e.g., Poisson-Quinton and LePage[18]).

From the above-mentioned works, it was found that tangential blowing was effective in suppressing boundary layer separation. However, its application to controlling dynamic stall on oscillating aerofoils has yet to examined in detail. Thus, the success (or lack of success) in controlling DS has still to be fully understood in order to be able to predict the merits of such control approach for other conditions [19]. Published research has mostly focused on the direct effect of the active flow control on the aerodynamic forces (lift, drag) acting on the aerofoil, e.g. [14, 19]. This is of course of highly important, but the flow structures linking the blowing at the leading edge of the aerofoil to the change which in the overall pressure and skin friction forces acting on the aerofoil are still to be better understood. This is where this study comes, using high-fidelity computational fluid dynamics (CFD) along with experimental results to shed more light on those structures and drive conclusions linking the change in the flow structures with the change in the aerodynamic forces acting on the aerofoil.

Numerous experimental, theoretical, and computational studies have been conducted to better understand the physics of dynamic stall. Gardner experimentally investigated high-pressure pulsed blowing for dynamic stall control on OA209 aerofoil. The best pulsed blowing was found as effective as constant blowing with the same mass flux for the control of dynamic stall [20]. Müller-Vahl experimentally explored leading-edge blowing for load control in wind turbine blade. On the other hand, mid-chord slot blowing was only effective for trailing-edge stall and not leading-edge one [21]. A method of "adaptive blowing" was successfully tested on a NACA 0018 aerofoil model at Reynolds numbers ranging from 150k to 500k[22].

As far as we are aware only few studies have performed CFD simulations on dynamic stall and control of leading-edge blowing. Qijun et al. numerically investigated the effects of synthetic jet control on unsteady dynamic stall for a rotor profile [23]. Spentzos et al. studied rectangular wings of NACA 0012 and NACA 0015 profiles to compare against experimental data [24]. Hutomo used SST k-ω RANS to study dynamic stall occurring in a Darrieus turbine [25]. Jain et al. validated high-resolution CFD predictions of static and dynamic stall of a finite span ONERA OA209 wing against the wind tunnel test measurements [26]. Chengyong et al. used unsteady RANS simulations to study the dynamic stall of the NREL S809 aerofoil with and without rectangular vortical generators, suggesting they can be effective in controlling the dynamic [27]. Ullah et al. explored passive flow control via leading-edge (LE) slats to reduce the dynamic stall (DS) phenomenon and related blade-wake interaction in an H-Darrieus type vertical axis wind turbine (VAWT) operating under low wind speed conditions [28].

Experimental wind tunnel tests have proven to be reliable tools in predicting the effect of steady blowing at the leading edge of the oscillating aerofoil e.g., [8]. Such results will be used in this study to enhance the confidence and understanding of the CFD analysis carried in this study. High fidelity CFD for aerofoils can range from Reynolds Averaged Navier–Stokes (RANS) to Large Eddy Simulation (LES) (or a combination of RANS and LES) and Direct Numerical Simulation, where the computational cost increases respectively. This study has used the RANS and Unsteady RANS approaches extensively while relying on experimental wind tunnel results for validation. Hence, a computational cost-effective approach has been pursued to investigate a range of conditions as applicable for wind turbines.

The focus is on the VAWT's blade that inherently shows dynamic stall due to the way that VAWT operates. Hence, the symmetric profile NACA0018 has been investigated, following previous VAWT studies of such profile for the effects of passive flow control, e.g., of micro vortex generators [29], Gurney flap [30] and leading-edge serration [31]. As in those studies, the focus in this study is on the small VAWT of a few kW, where the blade profile experiences aerodynamics dominated by a laminar boundary layer, i.e., the Reynolds number as based on the chord length is lower than 400k. Such blade profile is prone to early stall due to the sensitivity of the laminar boundary layer to adverse pressure gradient, making a control method as a steady blowing at the leading edge even more attractive to delay dynamic stall.

This study is organized to give an overview of the numerical simulation using a commercial CFD package, ANSYS Fluent, as an accurate, time efficient and economical way of simulating an oscillating NACA0018, by actually oscillating the freestream direction over a stationary NACA0018 aerofoil for a range of frequencies with different leading edge blowing control parameters. Computational results are compared with known experimental static and oscillating NACA0018 aerofoils. Finally, the behaviour of the vorticity fields, velocity profiles and aerodynamic coefficients are provided in detail to examine the links between the leading-edge blowing momentum, the oscillation frequencies of the aerofoil and the forces acting on the aerofoil.

2. Methods

2.1 Experimental approach

The wind tunnel experiment of Muller et al [8] is used to provide experimental results for the NACA 0018 aerofoil model [8]. That model was equipped with two blowing slots on the upper surface, positioned at 5% and 50% of the chord length (refer to Figure 1(b)). It should be noted that the experimental results used for this study did not utilise the second blowing slot located near the mid-chord of the aerofoil, i.e., that slot was blocked.

These slots point at a 20° angle toward the trailing edge of the aerofoil. The aerofoil model had span b = 0.610 m and chord length c = 0.347 m, and the slot height of the as-designed model was 1.2 mm. In the experiments chosen for comparison, the Reynolds number was Re_C = 250k and freestream M = 0.03265 (corresponding to a freestream velocity of U_∞ = 11.1 m/s). Hence, the aerofoil was dominated by a laminar boundary layer aerodynamics [29].

A total of 40 pressure taps were strategically positioned along both the upper and lower surfaces of the model. These pressure taps served the purpose of acquiring experimental pressure coefficient (C_p) values, which were utilized in the calculation of the corresponding experimental lift coefficient (C_L) values.

The momentum coefficient $C\mu$, defined by

$$C_\mu = \frac{hU_j^2}{\left(\frac{1}{2}\right) cU_\infty^2} \quad (1)$$

which is a measure of the effect of blowing. In Eq. (1), h is the slot height, U_j is the jet blowing velocity, c is the aerofoil chord, and U_∞ is the freestream velocity. Further details on the experimental methodology are provided in Muller at al [8].

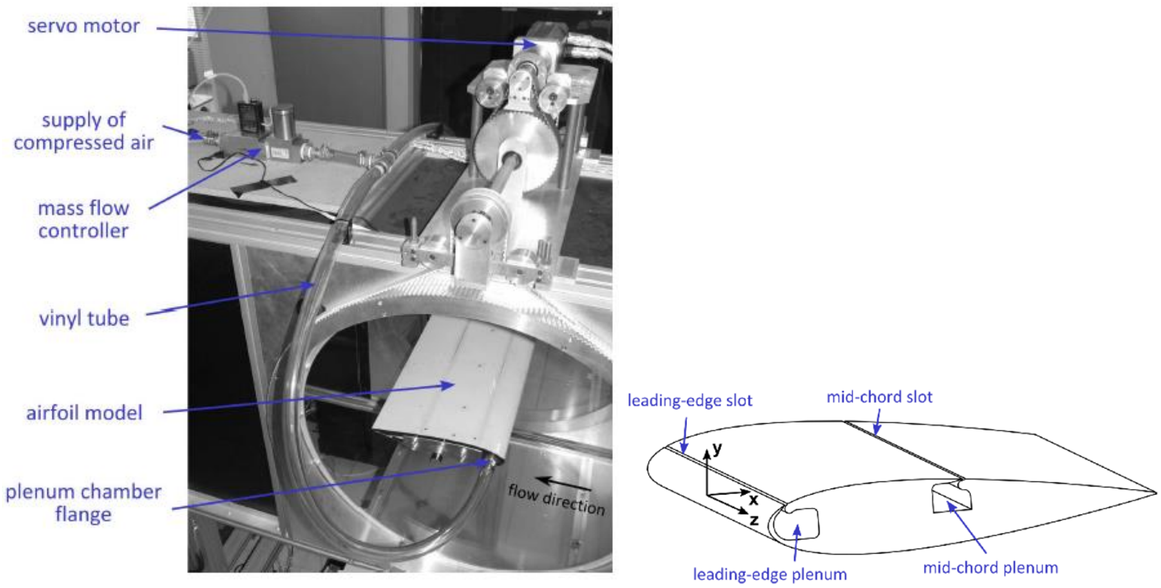

(a) (b)

Figure 1. Experimental setup (a) and NACA 0018 aerofoil model with two blowing slots (b) [8] (reproduced from ref [8] with permission)

2.2 Computational method

2.2.1 Static simulation

RANS Calculations were performed over static condition of the incoming speed and a stationary NACA 0018 aerofoil with a leading-edge blowing mimicking the static experimental conditions. A computational C domain was used as illustrated in Figure 2, showing the whole 2D computational domain and close-up view of this grid together with the situation of the blowing slot on the aerofoil. The grid extends from −10 chords upstream to 20 chords downstream and the upper and lower boundary extend 10 chords from the profile.

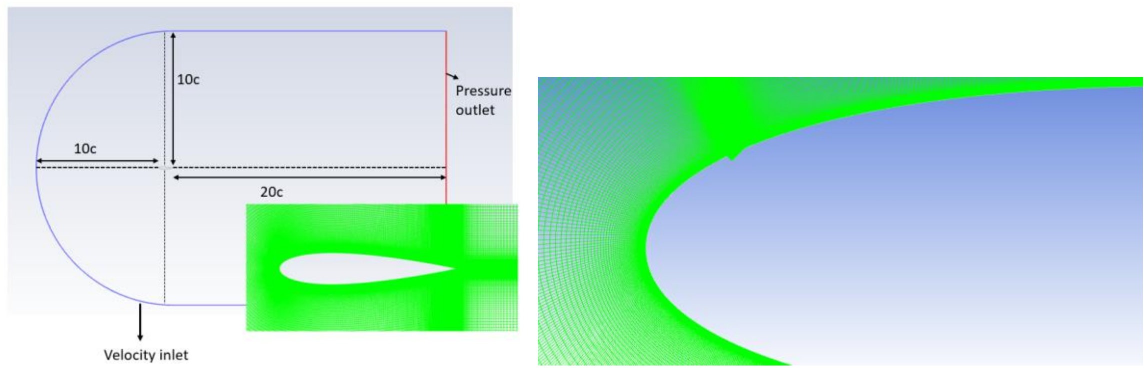

Figure 2. C-type mesh around NACA 0018 aerofoil and aerofoil with leading-edge blowing slot

The present study employed the commercial RANS-based code FLUENT, which offers a range of fully turbulent and transport equation-based transition models. Specifically, the Spalart-

Allmaras and the low Reynolds k-w SST turbulence models, as well as the k–kL–ω and k–ω SST transition models, were explored. These models were applied to both clean aerofoil configurations and aerofoils equipped with leading edge control mechanisms. Through a systematic examination of these models, it was observed that the Transition SST model yielded better agreement with experimental data for the clean aerofoil, while the Spalart-Allmaras module exhibited improved compatibility with the aerofoil featuring leading edge control configurations. Such comparative analyses between numerical results and experimental data can provide confidence in the accuracy and reliability of the employed CFD solvers. In the simulations, second order upwind discretization in space is used, and the resulting system of equations is then solved using the SIMPLE coupled solution procedure. Inflow velocity condition was imposed along with a pressure outlet as an outflow condition. No slip boundary conditions were imposed on the aerofoil's surface and the flow was assumed to be incompressible.

As accurate prediction of transition necessitates good resolution in the boundary layer, the wall coordinates y+ of the first grid point off the body is ensured to be less than 1. Different sized grids are used to ensure grid independence of the calculated results. This is achieved by obtaining solutions with an increasing number of grid nodes until a stage is reached where the solution exhibits negligible change with a further increase in the number of nodes. Consequently, the grid size giving the grid independent results are selected.

In this study, for clean aerofoil, different sized grids with 145k, 328k and 741k nodes were used to ensure grid independence of the calculated results. In the situation of aerofoil with C_u=2.6% leading blowing control, the test grids were 146k, 330k and 745k respectively. In Table 1, the distribution of numerical data obtained from the models and experimental data in terms of lift and drag coefficients at α=4° versus grid size are given. Fig.3(a) and Fig.3(b) show the distribution of the friction coefficient (Cf) and the pressure coefficient (Cp) over the NACA 0018 aerofoil. Particularly, when the grid numbers are increasing, the C_L and C_D show little difference and the resulting curves exhibit a high degree of overlap and similarity. Hence, by comparing the results in Table 1 and examining Figure 3, we chose the mesh number 145k for clean aerofoil simulation and 146k for leading-edge control simulation, as it predicts well the aerodynamic performance, while offering reduced computational cost.

Table 1. The lift and drag coefficients of the baseline and Cu=2.6% at α =4° versus grid size based on the transition models.

α =4°	EXP.	Mesh Number(baseline)			α =4°	EXP.	Mesh Number (Cu=2.6%)		
		145000	328000	741000			146000	330000	745000
C_L	0.3994	0.3732	0.3725	0.3694	C_L	0.5071	0.5450	0.5484	0.5561
C_D	0.03340	0.01798	0.01958	0.01823	C_D	0.02186	0.02683	0.02683	0.02712

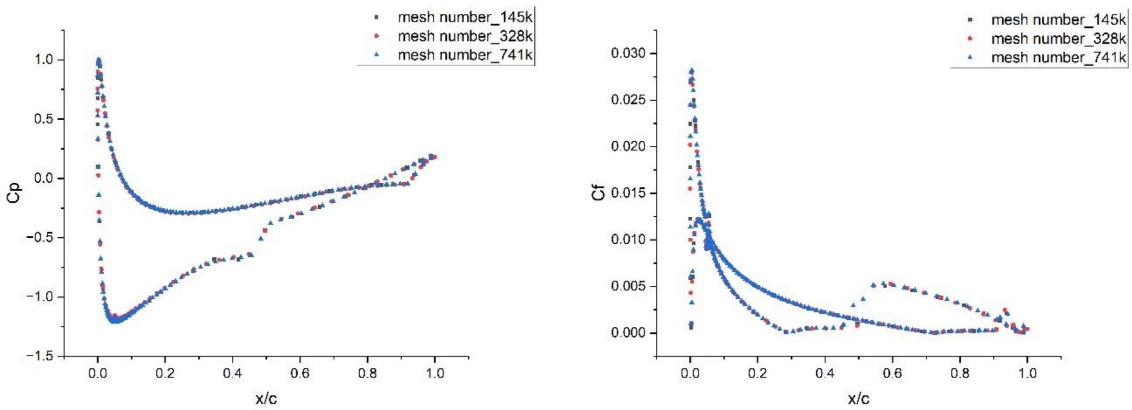

(a) (b)

Figure 3. The distribution of pressure coefficient(a), skin friction coefficient(b) over the NACA 0018 aerofoil at α =4° versus grid size based on the transition SST model

2.2.2 Dynamic simulation

Dynamic conditions on the blade of a lift-based vertical kinetic turbine as VAWT are caused by the fundamental operation of the turbine. This can be illustrated by looking at the straight H VAWT, where the angle of attack (AoA) α experienced by the blade can be written as $\tan(\alpha) = \frac{\sin(\psi)}{[TSR+\cos(\psi)]}$. The flow angle $0 < \psi < 2\pi$ is between the wind velocity vector and the profile chord line (the profile leading edge points into the wind at $\psi = 0$). The tip speed ratio $TSR = \frac{\Omega R}{U}$, where Ω is the turbine's rotational speed, R is the radius of the rotor and U is the wind speed [30]. It is clear that for low and moderate TSR, the AoA can periodically achieve high values as the flow angles oscillates between 0 to 2π, leading to dynamic stall (DS) conditions. Obviously, the wind velocity vector can also vary in time and magnitude adding further unsteadiness to the DS, but in this study, we focus on the fundamental periodic change in the AoA that can lead to DS.

The URANS, Unsteady Reynolds Average Navier Stokes approach is a relatively inexpensive computational approach to analyse flows with periodically varying conditions, e.g [31]. URANS model has shown good overall agreement with experimental data for VAWT [29], [31], and will serve as the computational tool in this study to investigate dynamic stall of the symmetric aerofoil NACA0018 that is commonly used for VAWT applications.

In this study, the investigated range of the angle of attack (AoA) spans from 0 to 20 degrees. During the pitch up phase, the angle progressively increases from 0 to 20 degrees, while during the pitch-down phase, the angle gradually decreases from 20 to 0 degrees. This mimics the conditions of a VAWT with a moderate TSR. However, the rotational speed of which the AoA varies is also important. This is done by oscillating the freestream over a stationary aerofoil while having a reduced frequency k defined as follows.

$$k = \frac{(\omega c)}{2U_\infty}, \tag{2}$$

where

$$\omega = 2\pi f\,, \tag{3}$$

and f is the oscillation frequency. In the pitch up phase, we take the AoA varying as (in rads):

$$\alpha = \omega t\,, \tag{4}$$

And in the pitch down phase:

$$\alpha = 20 * \frac{\pi}{180} - \omega t. \tag{5}$$

Inflow conditions

The time varying inflow velocity conditions are defined during the pitch up phase as:

$$V_x = U_\infty * \cos(\omega t)\,, V_y = U_\infty * \sin(\omega t)\,, \tag{6}$$

and in pitch down:

$$V_x = U_\infty * \cos(20 * \pi/180 - \omega t)\,, V_y = U_\infty * \sin(20 * \pi/180 - \omega t)\,. \tag{7}$$

The x direction aligns with the profile's chord line and the y direction is normal to it.

Grid generation

Like the static simulation, a C grid layout was adopted, and different cell sizes for a quadratic mesh have been used to pursue grid independence in the aerodynamic forces. The grid details are given in Table 2. The Δy+ spacing of the first grid point off the wall was less than 1 for all grid levels. The mesh contained around 145k, 328k and 741k cells respectively. Each successively finer level was created by increasing 1.5 times the grid points in each coordinate direction from the coarser grid. Along the aerofoil about 320, 480 and 720 grid points were distributed with a high resolution near the leading and trailing edges. In addition, triangular cells with high flexibility to adapt to complex geometry placed in the jet domain as part of the blowing control mechanism. Inside the aerofoil slots, the walls boundary layers were neglected, so inviscid wall were specified inside the slot to ease the computational load calculation and the calculation of the momentum coefficient Cμ (see Eq (1)). Nevertheless, A fine grid spacing in the order of 0.0001c – 0.001c was used inside of the slot. Mesh independence tests showed little difference in terms of the aerodynamic forces and thus the mesh of 145k cells was chosen as the main mesh for the simulations.

Table 2. Different grid information

Overall grid size	Δy+	Number of grid points along aerofoil	Grid size at the x and y directions
145424	0.8	320	977*150
328384	0.53	480	1467*225
741400	0.36	720	2201*338

Fig 4 shows the variations of the lift and drag coefficients with the angle of attack when using various URANS models and experimental results during pitch up for Re_C=250k. Note that the experiment yielded a somewhat unusual lift curve shape. Rather than an approximately linear variation of the lift with the angle of attack over the lower angles, the experimental results exhibit a nonlinear increase in lift between approximately 5 and 10 degrees. This is believed to be due to the presence of a laminar bubble near the aerofoil's upper surface leading edge, which caused an additional flow acceleration around it. The transition SST k-omega URANS model is the one able to capture this effect. However, the Spalart-Allmaras (SA) model also in overall gives similar accuracy as the transition SST model, while the RSM model significantly overpredicts lift at high angle of attack.

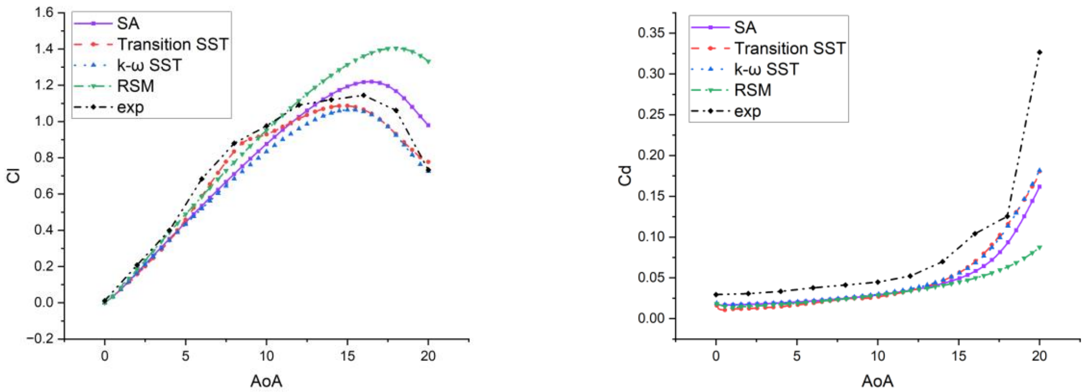

Figure 4. Lift and drag coefficients variations with angle of attack for oscillating NACA0018 aerofoil using various URANS models and the experimental results, k=0.0078, Re=250k

The pressure distributions in Figure 5 are also based on the 145424 grid size. The simulation results match well with the experimental data for most of the cases. For where massive flow separation is present in the flow, such as at α=20°, the pressure distributions do not agree as much, but the overall pattern of the pressure distribution is still reasonably well.

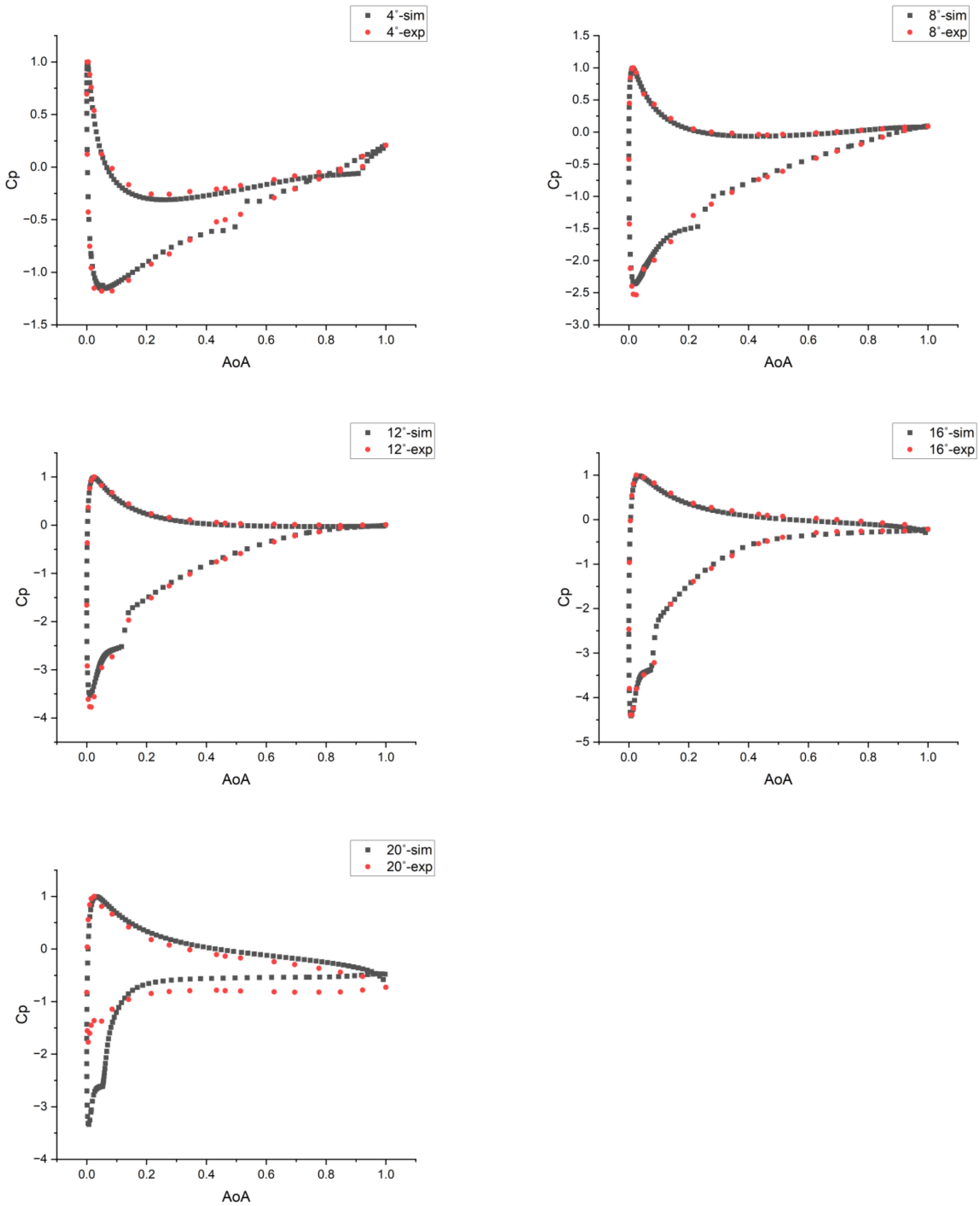

Figure 5. Pressure coefficient distributions along the aerofoil's chord line for different angle of attack where the SST URANS model was used for the simulation. x/c =(0,1) correspond to the leading and trailing edges respectively and the rest of the conditions are as of Fig 4.

Simulation setup

We reproduced the experimental quasi-static NACA0018 pitching aerofoil cases studied by Muller-Vahl[8]. The transition SST model demonstrated substantially better results for lift and drag coefficients for clean aerofoil. In the case with the leading-edge control, the Spalart-Allmaras (S-A) model fits better with the experiment results. This follows other studies supporting the use of the S-A model for injection and leakage flows, e.g. [32]. For the rest of the simulations of high reduced frequencies and leading-edge blowing controls, there were no data found in the literature for comparison. Hence the SA model was used for the URANS simulations of the dynamic case.

The numerical simulation was set up using a time-implicit marching segregated solver using the SIMPLE algorithm. For spatial discretization, a second-order upwind finite-volume scheme was applied for the convection terms and a second-order central finite-volume scheme was used for the diffusion term. Since the time step size is a crucial parameter for unsteady cases, depending on the amplitude, frequency and the far field velocity, a few of time-step refinements has been employed to ensure the temporal accuracy of the results [33]. An example of the time step size independence test for aerofoil with leading-edge control Cu=2.6% under k=0.0078 can be seen in Figure 6. There is almost no effect on the numerical result by the chosen time steps. The agreement between the simulation and the experiment is good for low angle of attack, but divergence is observed for the drag at high angle of attack where the URANS underpredicts.

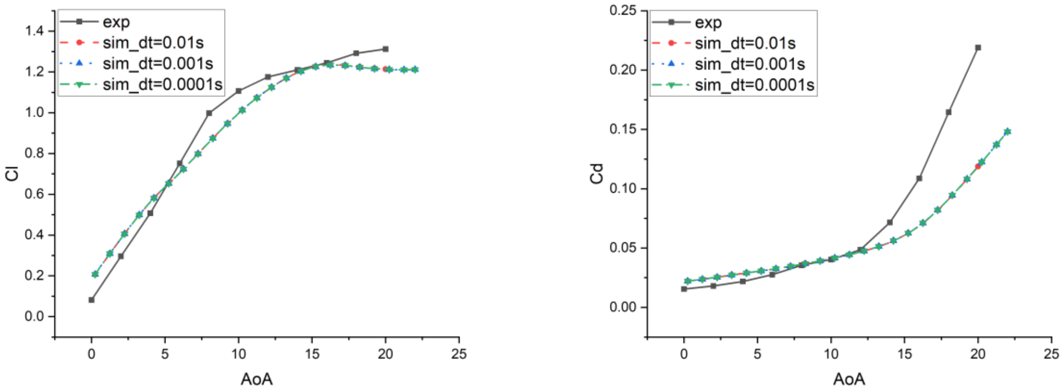

Figure 6. Time step size independence test for aerofoil with leading-edge control Cu=2.6%, k=0.0078

3. Results and discussion

Static case- Effect of blowing momentum coefficient on static stall

All the results are provided based on the simulation results. It is reminded that the lift coefficient is defined as $C_L = \frac{L}{\frac{1}{2}\rho U_\infty^2 C}$ where L is the lift force. The drag coefficient is similarly defined as $C_D = \frac{D}{\frac{1}{2}\rho U_\infty^2 C}$ where D is the drag force. The incompressible pressure coefficient is defined as $C_p = \frac{p - p_\infty}{\frac{1}{2}\rho U_\infty^2}$.

Figure 7 presents a comprehensive comparison between experimental results and numerical calculations of lift and drag coefficients as a function of angle of attack for both a clean aerofoil and an aerofoil incorporating the leading edge blowing control. The solid lines in the graph represent the experimental data, while the dashed lines correspond to the simulation's time-averaged results.

Notably, the computational lift and drag coefficients exhibit a satisfactory agreement with the experimental data when the angle of attack is below 16°. However, as the aerofoil approaches the stall angle, the numerical models consistently underestimate the experimental values. This discrepancy can be attributed to the increasing flow separation above the upper surface of the aerofoil, leading to stall and post-stall conditions. Consequently, the effectiveness of the employed numerical turbulence models can deteriorate in accuracy when capturing these complex flow phenomena.

Nevertheless, Figure 7 illustrates the significant impact of leading-edge slot steady blowing on the aerodynamic performance of the aerofoil, contingent upon the momentum coefficient. At angles of attack prior to stall, blowing with sufficiently high Cu values yields lift coefficients that far surpass baseline values. Specifically, blowing with Cu=5.4% generates an increase in lift coefficient (ΔC_L) of over 0.5 within the range of 9 deg < AoA < 20 deg. The qualitative effect of control with Cu=2.6% aligns with that of 5.4%. However, the degree of lift coefficient improvement is very limited, especially at small AoA. The reason could be that under this momentum of injection, the blowing speed is almost the same with freestream velocity, so it did not have big difference for the flow field. As the angle of attack exceeds 15°, the influence of blowing control becomes more pronounced. In contrast to the stall delay observed with high momentum coefficients, when the jet speed is lower than the freestream speed (as demonstrated by the Cu=0.5% curve), stall occurs earlier, leading to a decline in the lift coefficient and an increase in the drag coefficient.

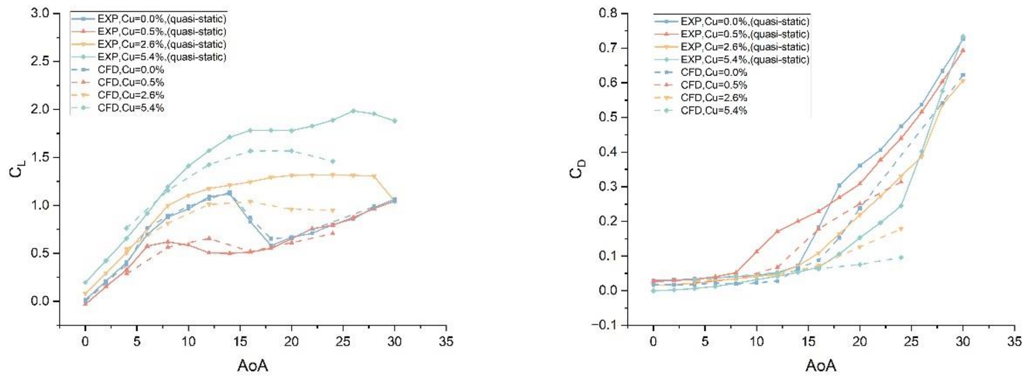

Figure 7. Aerofoil performance at different angles of attack under different control momentum, lift coefficient (left) and drag coefficient (right)

Figure 8 provides a visualization of the wall velocity gradient at different locations. Specifically, for α=4°, we have chosen x/c=0.4, 0.5, and 0.6 for analysis. For α=12° and 16°, x/c=0.1, 0.2, and 0.3 were selected. The reason behind these choices stems from observing the clean aerofoil pressure coefficient plot (Figure 5), which reveals the occurrence of laminar separation at these specific locations. The solid black lines represent the baseline case, while the red (dashed), blue (dotted), and green (dashed-dotted) lines depict the effects of leading-edge control with Cu values of 0.5%, 2.6%, and 5.4%, respectively. Notably, the shape of the boundary layer velocity profile exhibits minimal changes. However, it is worth noting that the velocity profile becomes slenderer and narrower when the location is closer to the blowing slot. Upon closer examination, it becomes evident that at α=16° and Cu=0.5%, the velocity at x/c=0.2 and 0.3 is significantly reduced, accompanied by an anomalous shape. This observation suggests that stall occurs at this stage, as indicated by the peculiar velocity behaviour.

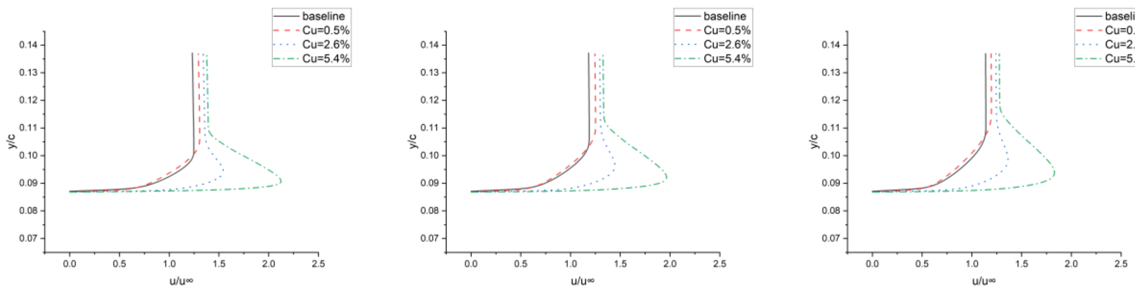

x/c=0.4 x/c=0.5 x/c=0.6

(a)

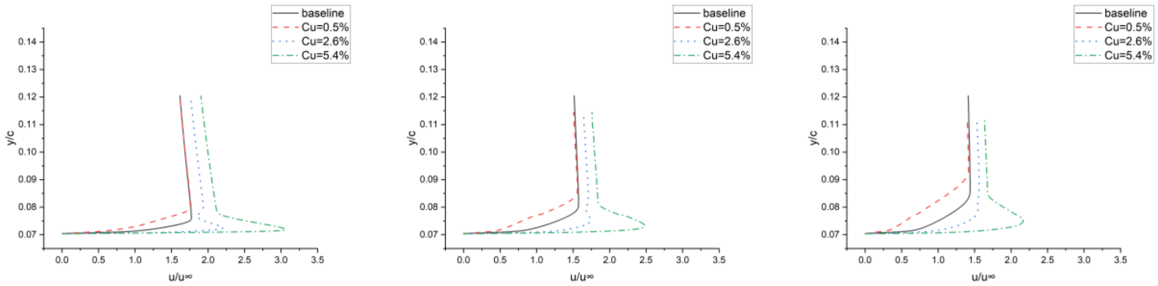

x/c=0.1 x/c=0.2 x/c=0.3

(b)

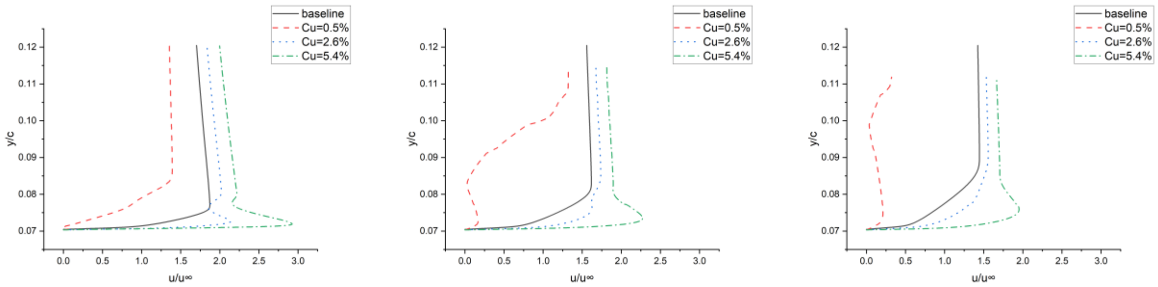

x/c=0.1 x/c=0.2 x/c=0.3

(c)

Figure 8. Numerical velocity profiles over the upper surface for α=4°(a),12°(b) and 16°(c) at different x/c location

In Figure 9, an interesting observation can be made regarding the baseline case. A distinct separation bubble is clearly visible above the suction side of the aerofoil, and as the angle of attack increases, the bubble gradually moves towards the leading edge of the aerofoil. However, in the case of the aerofoil with the leading edge blowing control, this phenomenon is not apparent. There are a couple of possible reasons for this:

1. As mentioned earlier, the baseline simulation employed the transition SST model, which effectively captures the transition effects within the separation bubble. On the other hand, the simulation for the aerofoil with blowing control utilized the Spalart-Allmaras model, which may not adequately capture this phenomenon. The choice of turbulence models can influence the accuracy in representing such flow phenomena.

2. It is anticipated that the blowing control has the effect of energizing the flow and mitigating the extent of the laminar separation bubble. This energetic influence on the flow caused by the blowing could potentially alter the behaviour of the separation bubble and diminish its visibility in the flow field.

Inspection of the pressure coefficient provides further explanation of the leading-edge blowing effect on C_L. The improved lift coefficient due to Cu=5.4% and Cu=2.6% is clearly seen by the wider area between the suction (upper) and pressure (lower) surface lines, while the decline in C_L for Cu=0.5% is also obvious. Therefore, similar to earlier work such as Huang et al. [34][35], the underlying blowing control mechanism is expected to be the suppression or postponement of the separation bubble and the reduction of the upper surface pressure coefficients to increase the lift and decrease the drag.

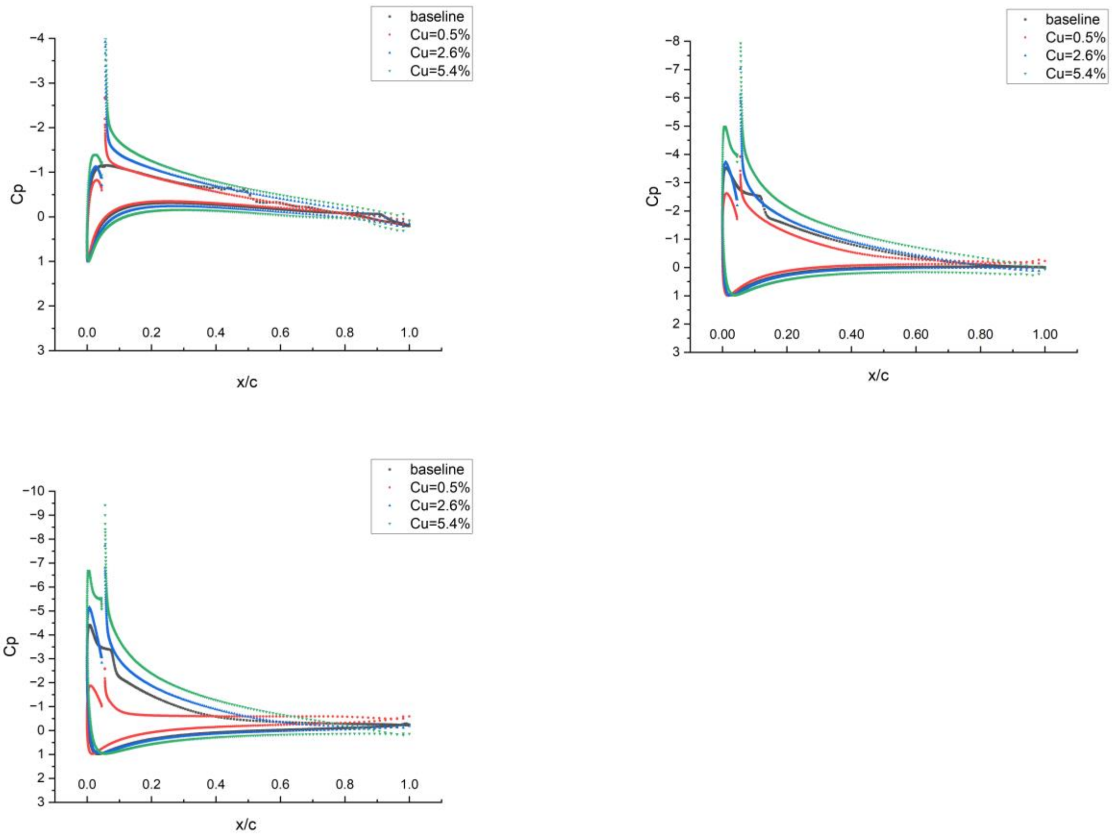

Figure 9. Comparison of pressure coefficient at α=4°,12°,16° for clean aerofoil and aerofoil under Cu=0.5%,2.6%,5.4% leading edge blowing control

The above discussion for pressures is further supported by the skin-friction coefficients as shown in Figure 10. It is observed that the larger leading edge control values of Cu=5.4% (green head-standing triangle) and 2.6% (blue triangle) exhibit higher skin friction coefficients, indicating more attached flow conditions compared to the smaller leading edge control Cu=0.5% and the clean aerofoil. Accordingly, the lower skin friction coefficient observed in the latter cases typically corresponds to separated flow regions, which contribute to lower lift coefficient values, as demonstrated in Figures 7 and 9, and also in Ref. [36].

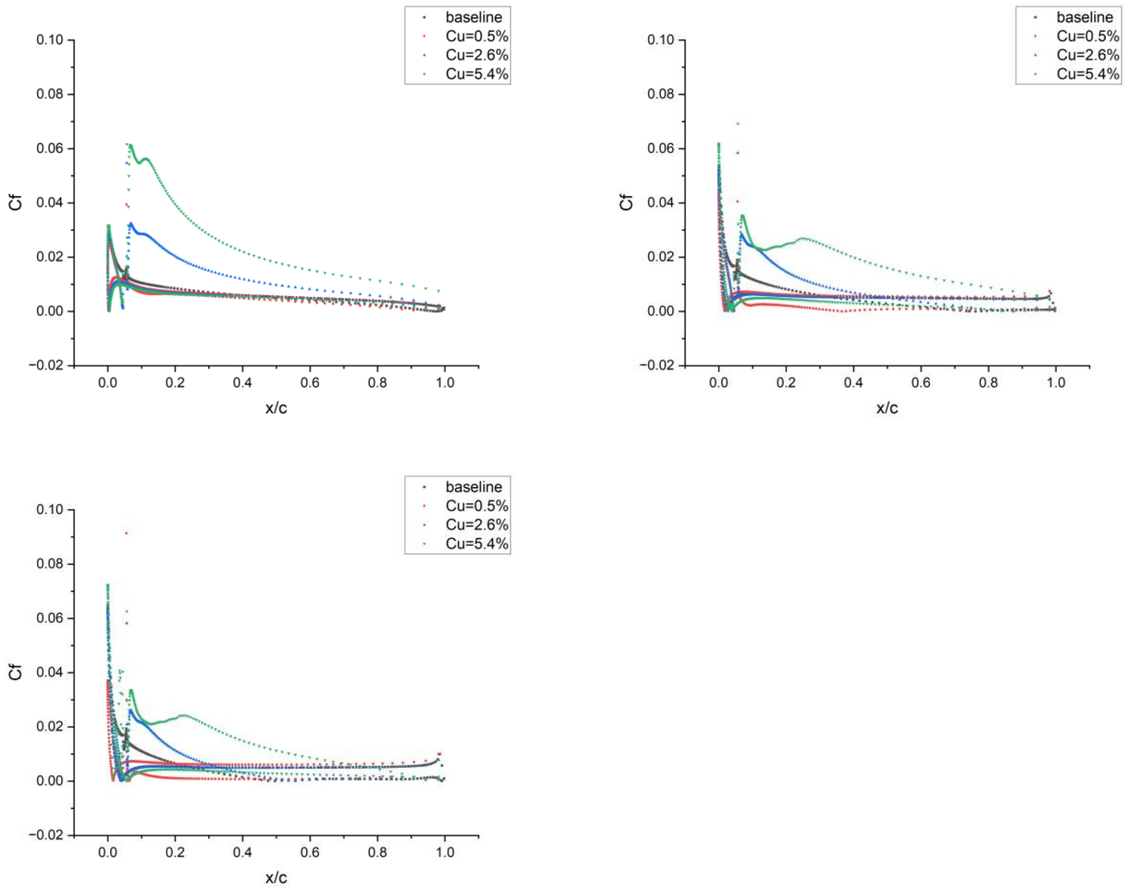

Figure 10. Comparison of skin friction coefficient at AoA=4°,12°,16° for clean aerofoil and aerofoil under Cu=0.5%,2.6%,5.4% leading edge blowing control

Figure 11 presents the streamlines and Z vorticity contour surrounding the NACA 0018 aerofoil at various angles of attack (α = 4°, 12°, and 16°) under different blowing control conditions. Notably, it can be observed that the presence of significant leading edge blowing momentum effectively suppresses trailing edge separation. This inhibitory effect becomes increasingly pronounced with a higher blowing momentum at the leading edge. On the contrary, when the jet momentum is reduced, such as in the case of Cu=0.5%, the blowing action promotes earlier stall. As depicted, the separation bubble moves closer to the leading edge of the aerofoil and extends over a larger suction region. The visual depiction in Figure 11 reinforces the significance of the leading-edge blowing control in modulating flow separation and highlights the contrasting effects observed at different blowing momentum levels.

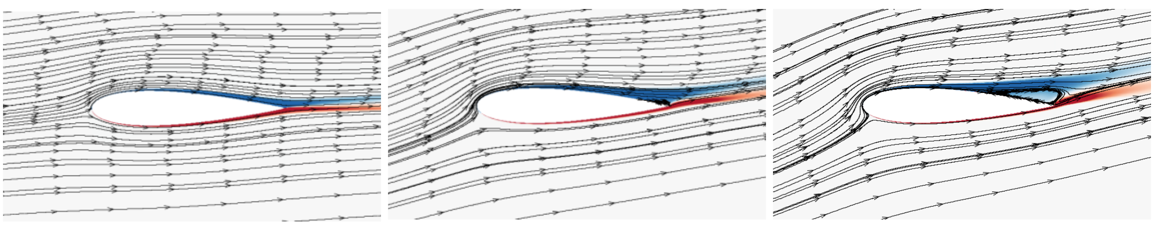

(a)

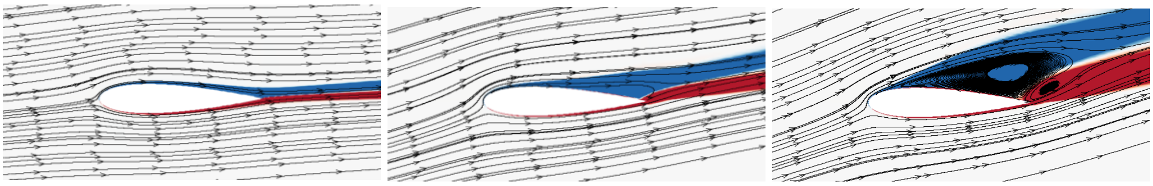

(b)

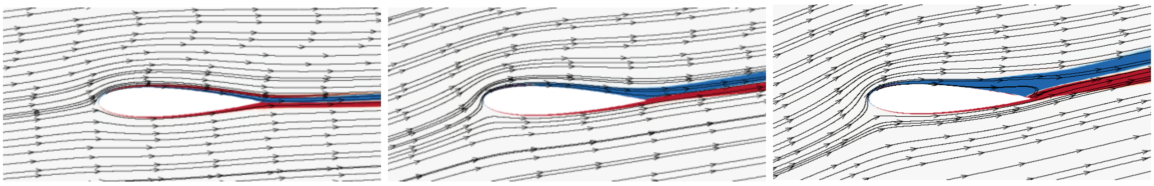

(c)

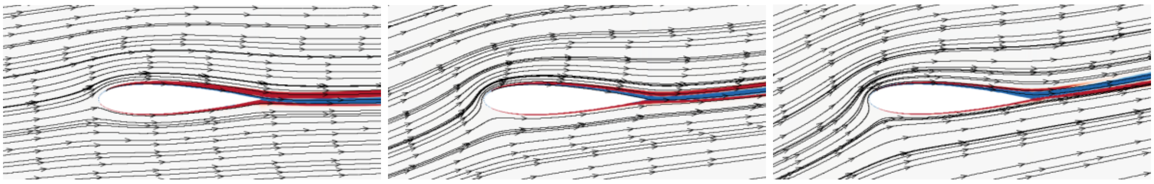

(d)

Figure 11. The streamline and the Z vorticity distribution at α=4°,12°,16° with different blowing control momentum (a) baseline (b) Cu=0.5% (c)Cu=2.6% (d) Cu=5.4%

Dynamic case

Figure 12 displays the simulated aerodynamic coefficients during dynamic stall conditions with varying reduced frequencies (k) of 0.0078, 0.1, and 0.2, at a Reynolds number (Re_C) of 250k. Notably, as the reduced frequency increases, there is an observable amplification in the disparity between the pitch up and pitch down values. This leads to broader loops and a noticeable alteration in the overall shape of the loops. The changes in the aerodynamic coefficients reflect the dynamic response of the system under different reduced frequencies, highlighting the influence of this parameter on the aerodynamic behaviour during dynamic stall.

Special attention is given on the aerodynamic coefficients' drop incidence delay in comparison with a static case [37]. Regarding the clean aerofoil, when the reduced frequency (k) is set at 0.0078, the lift curves exhibit linearity up to an angle of attack (α) of approximately 15°, where the most pronounced disparities in lift values occur. At angles of attack near 15°, adverse pressure gradients induce reversed and separated flow in the vicinity of the trailing edge. However, when k is increased to 0.1 and 0.2, the lift curves exhibit linearity up to α = 20°, suggesting the absence of stall phenomena. This behaviour is attributed to the increased rotational speed resulting from the increased reduced frequency.

Similar observations can be made for the leading-edge blowing case with Cu=0.5%. Under different reduced frequencies, stall angles are identified as α = 11°, 12.5°, and 15°, respectively. The incidence delay is found to be higher with an increasing reduced frequency. The unsteady conditions yield maximum lift coefficients higher than of the steady condition. However, this effect is less prominent for aerofoils equipped with Cu=2.6% and 5.4% blowing control. Consequently, it can be concluded that leading edge control mitigates the impact of rotation to some extent, suggesting a counteracting effect.

When increasing the reduced frequency, an intriguing observation can be made regarding the growth rate of the lift coefficient during the pitch up stage. It becomes apparent that the rate of increase in the lift coefficient diminishes as compared to lower reduced frequencies. Conversely, during the pitch down stage, a distinct pattern emerges. Specifically, when considering cases such as Cu=5.4% at $\alpha \leqslant 12°$ and Cu=2.6% at $\alpha \leqslant 10°$, the lift coefficient values at these angles of attack surpass those observed during the pitch up stage. This behaviour can be attributed to the influence of rotational inertia. The rapid rotation speed maintains the flow field from the preceding moment, resulting in an impact on the subsequent flow field. During the pitch down process, the reattachment of the boundary layer experiences a delay at lower angles of incidence compared to the static aerofoil configuration. This delay induces a hysteresis loop in the evolution of the aerodynamic coefficients. Over time, the lift and drag coefficients gradually recover the values attained during the pitch up phase.

Drag coefficient evolutions are similar until a critical angle of attack (AoA) for which the drag coefficient of the pitching cases increases in a significant manner compared to the static case. This critical AoA depends on the reduced frequency. The higher the reduced frequency value, the higher this critical AoA is. Similar to the lift coefficient, the drag coefficient evolution in the pitching cases shows a hysteresis phenomenon.

These findings shed light on the intricate interplay between reduced frequency, leading-edge control, and the resulting aerodynamic behaviour. They further underscore the significance of unsteady conditions and the potential benefits offered by a leading-edge control in managing the impact of rotation on aerodynamic performance.

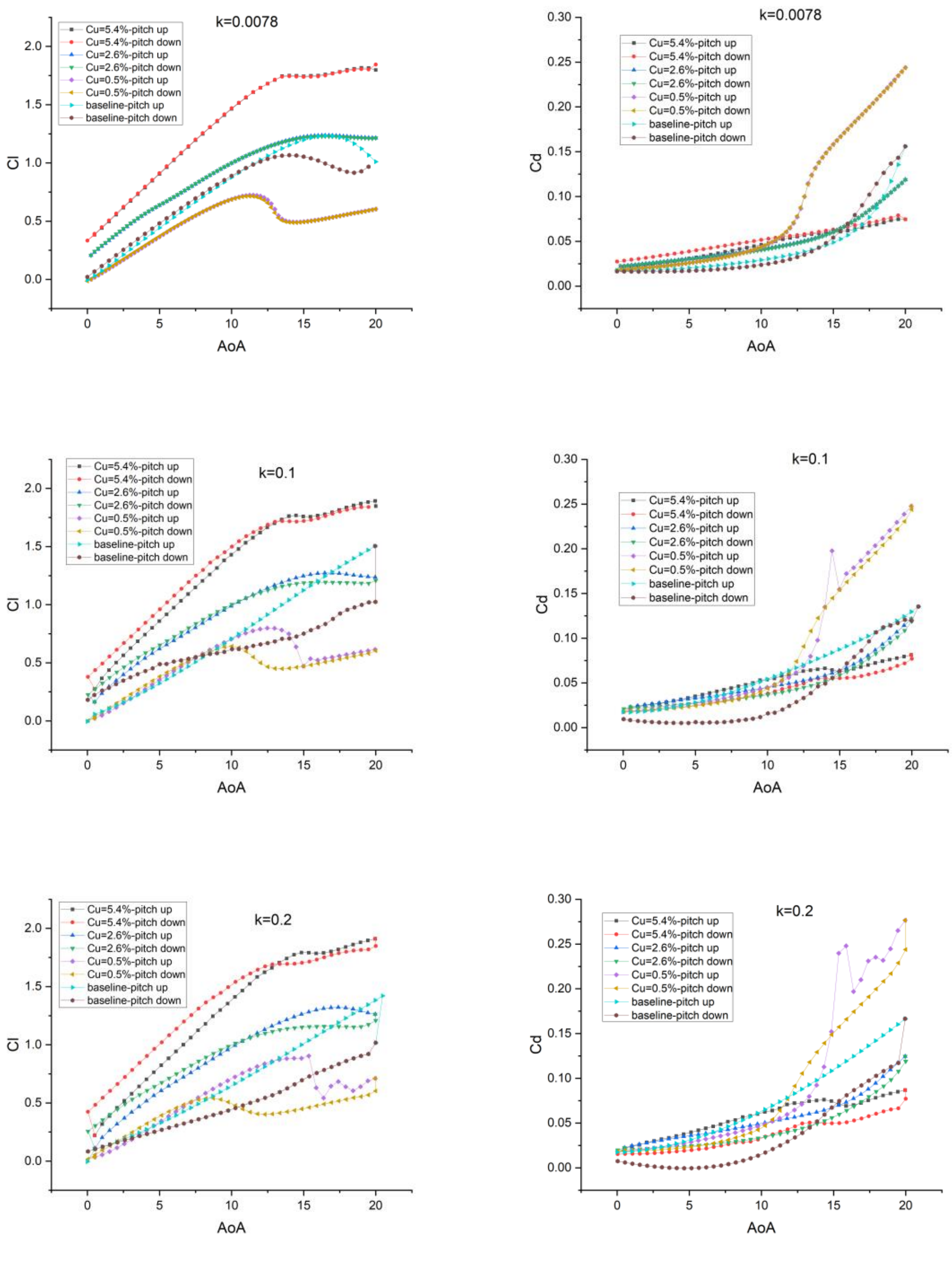

(a) (b)

Figure 12. Lift coefficient hysteresis loop (a); and (b) Drag coefficient hysteresis loop with different reduced frequency

Having the knowledge of the vorticity field of the pitch up and pitch down is helpful in linking the evolution of the phase-averaged lift and drag coefficients with the flow around the aerofoil, investigating the complexity of the boundary layer and vortex shedding during the dynamic flow condition. Figures 13 and 14 present the z-direction vorticity and streamlines around the aerofoil during the pitch up and pitch down phases at α=4°, 12°, and 16°, accompanied by corresponding x-velocity contour plots for k=0.0078. Although the angles of attack are the same, certain distinctions can be observed among the different cases. At an angle of attack of 12°, a minor trailing edge separation is apparent. As the angle of attack increases to 16°, the size of the separation bubbles becomes more pronounced. During the pitch up phase, the separation bubble encompasses approximately 40% of the suction side, while during the pitch down phase, this ratio increases to 50%. It is worth noting that the analysis was conducted using a reduced frequency value of k=0.0078, which corresponds to a relatively low rotational speed, almost a quasi-static simulation. Consequently, the observed differences are not as pronounced. Similar plots were generated for k=0.1 and k=0.2 and the effects become more discernible.

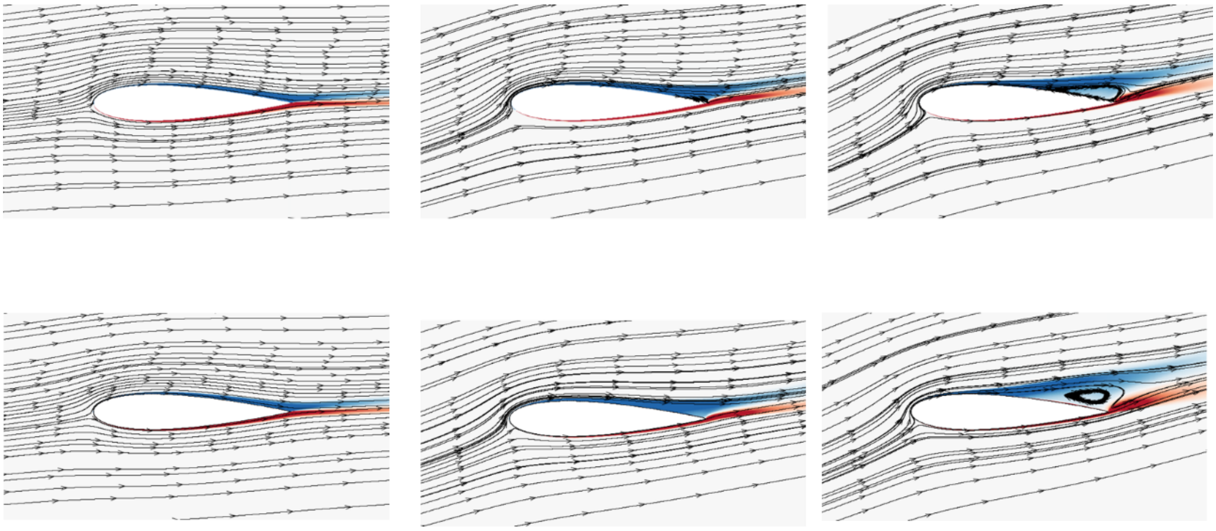

Figure 13. streamline and Z vorticity contour for clean aerofoil when k=0.0078, pitch up (upside) and down (downside) process, α=4° (left) ,12°(middle), 16°(right)

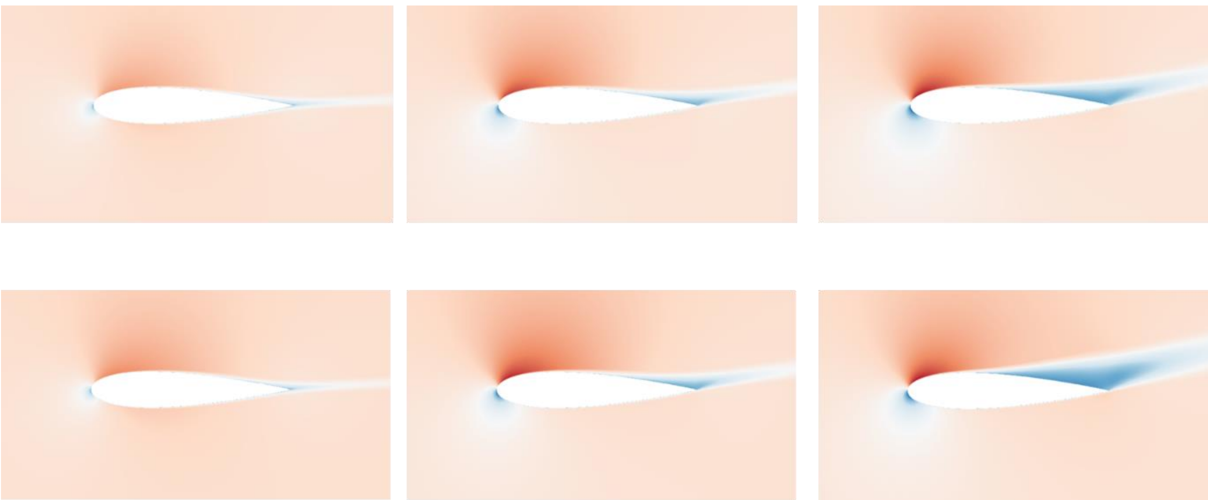

Figure 14. X velocity contour for clean aerofoil when k=0.0078, pitch up (upside) and down (downside) process, α=4° (left) ,12°(middle), 16°(right)

Figure 15 illustrates the z-direction vorticity and streamlines surrounding the aerofoil at an incidence of α=4° and 16° for different reduced frequency values: k=0.0078, 0.1, and 0.2. Figure 16 presents the corresponding x-velocity contour. These figures serve to enhance our comprehension of the influence of reduced frequency on the flow field. Notably, at α=16°, a distinct pattern emerges whereby the trailing edge separation bubble is progressively suppressed as the reduced frequency increases. Higher reduced frequencies correlate with smaller separation bubbles forming at the trailing edge, indicating a more favourable flow behaviour.

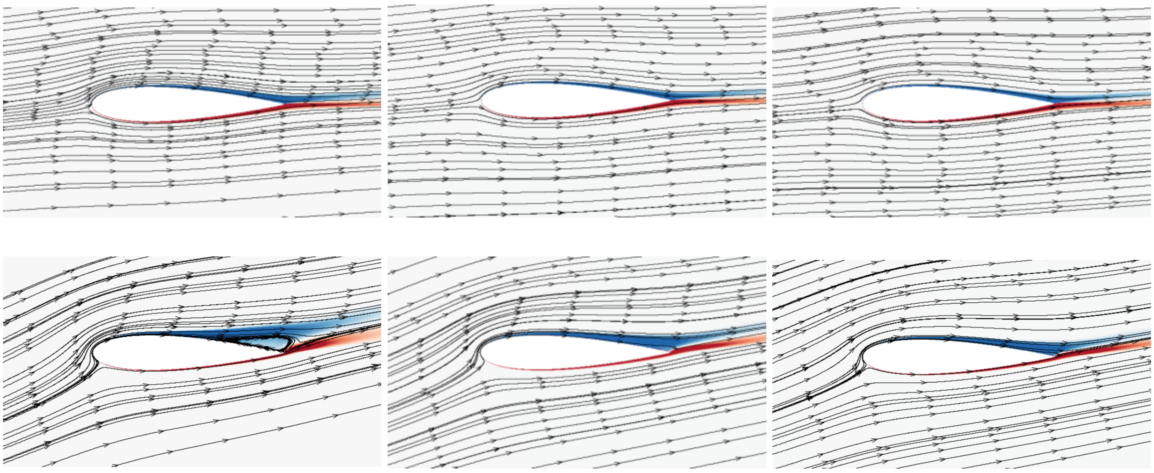

Figure 15. streamline and Z vorticity contour for clean aerofoil when k=0.0078 (left), k=0.1(middle), k=0.2(right), α=4˚(upside) and 16˚ (downside)

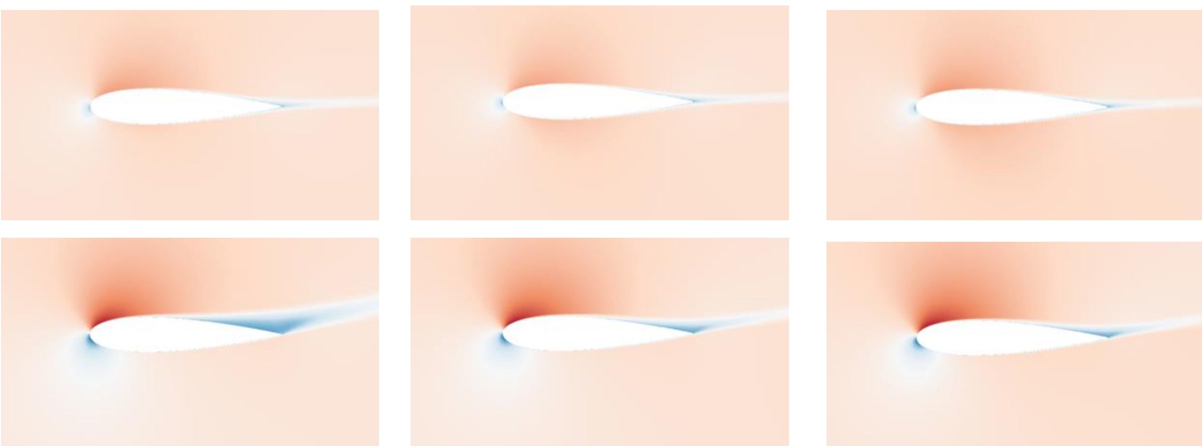

Figure 16. streamline and Z vorticity contour for clean aerofoil when k=0.0078 (left), k=0.1(middle), k=0.2(right), at α=4˚(upside) and 16˚ (downside)

Figure 17 showcases the streamline patterns and Z vorticity contours during the pitch-up process for an incidence angle of α=16°, comparing the cases of a clean aerofoil and an aerofoil with leading-edge blowing control (Cu=0.5%, 2.6%, and 5.4%) at two different reduced frequencies: k=0.0078 (left) and k=0.2 (right). The plot reveals the impact of blowing control on the aerofoil's flow field. When Cu is small, the blowing action actually facilitates the occurrence of laminar flow, leading to a larger trailing edge separation bubble. Conversely, when Cu is significantly larger, this measure effectively suppresses the occurrence of laminar flow at the trailing edge, validating our earlier observations in Figure 11.

Of particular note is the distinct influence of reduced frequency on the clean aerofoil. While the inhibitory effect on trailing edge bubbles is prominent in the baseline cases, it is comparatively weaker in cases with leading-edge control. This distinction is further corroborated by Figure 18, which demonstrates that for clean aerofoil during pitch up process at k=0.0078, the onset of trailing edge separation occurs at x/c=0.5, whereas for k=0.2, this location shifts to x/c=0.75. While during the pitch down process, we can clearly observe similar effects: when k=0.0078, the trailing edge separation initiates at x/c=0.35, whereas for k=0.2, this location shifts to x/c=0.2. The forward movement of the separation location is attributable to the increasing rotational speed, which accentuates the inertial effect and restricts the timely alteration of the flow field from its previous state. Notably, no significant changes in the trailing edge separation point are observed for Cu=0.5% and 2.6%, regardless of whether it is during the pitch up or pitch down process.

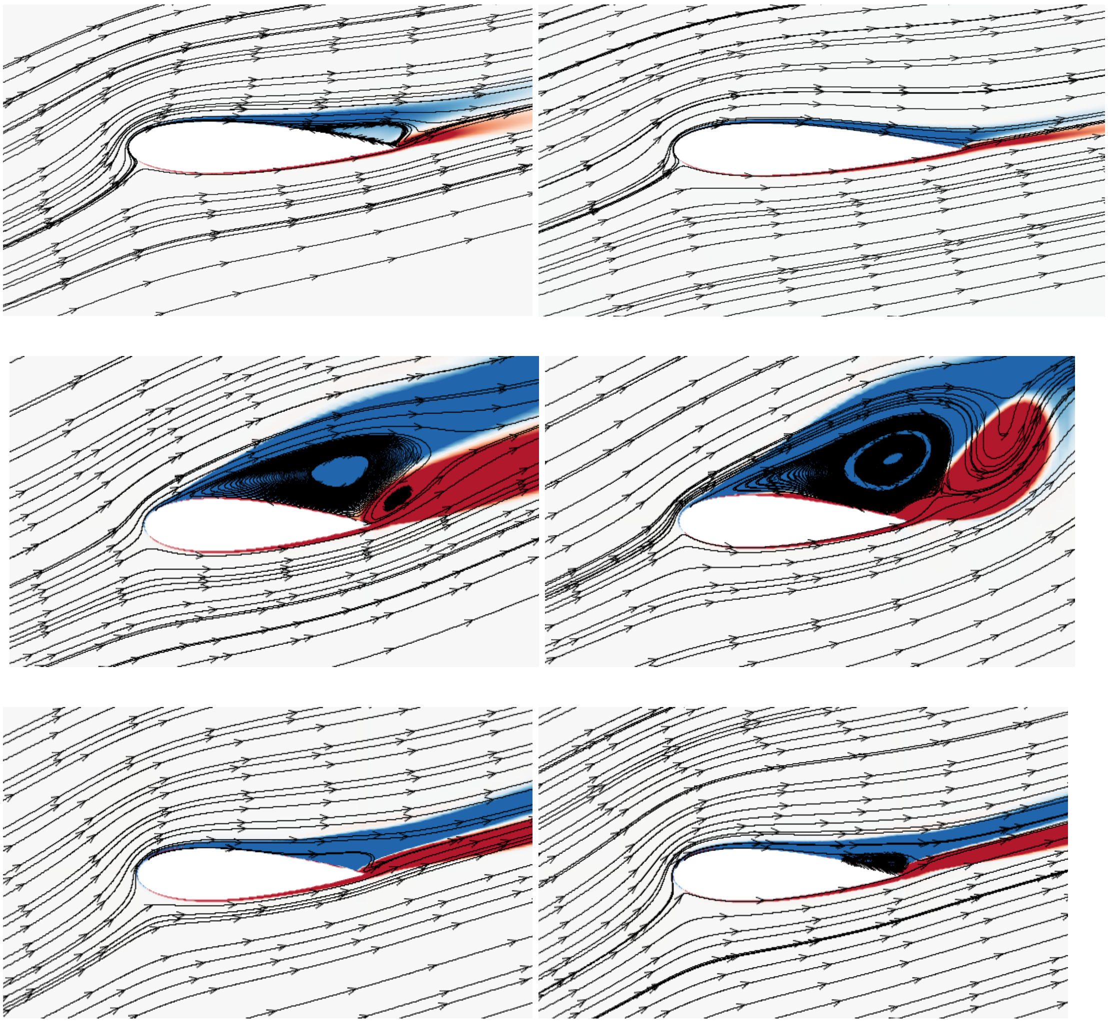

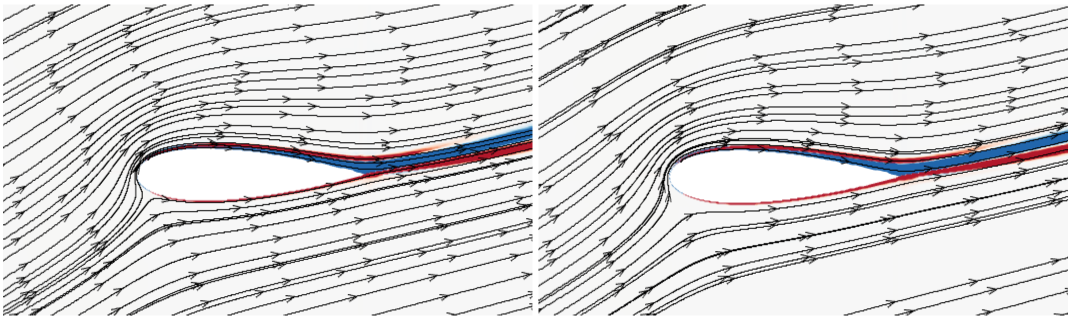

Figure 17. streamline and Z vorticity contour when k=0.0078(left) and k=0.2(right), α=16° for clean aerofoil and leading-edge blowing Cu=0.5%,2.6% and 5.4%, pitch up process

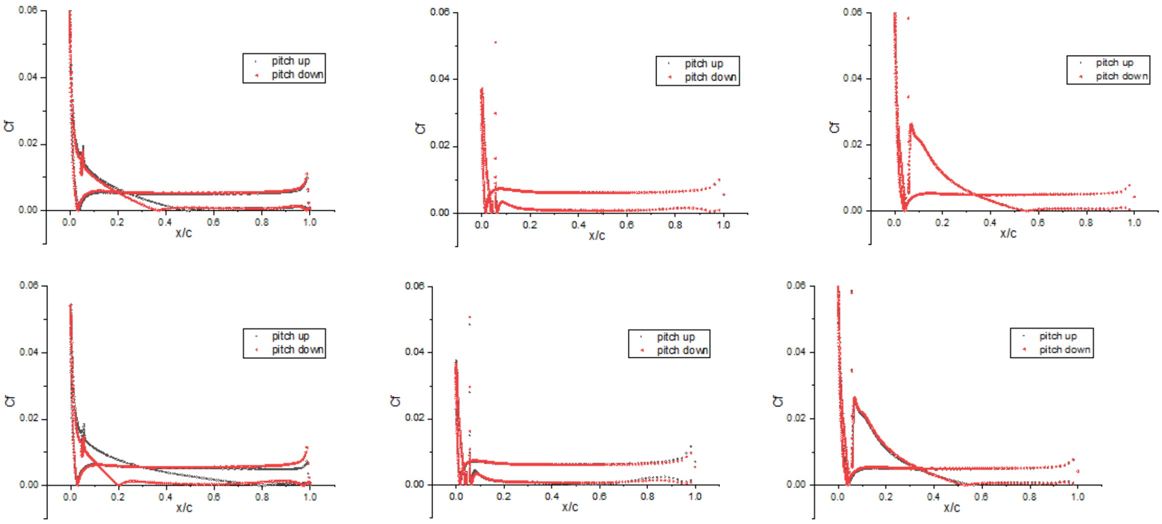

Figure 18. skin friction coefficient when k=0.0078(upside) and k=0.2(downside), α=16° for clean aerofoil and leading-edge blowing Cu=0.5% and 2.6% during pitch up and pitch down process

The investigation of trailing edge separation is conducted for various pitching cases, and the results are presented in Figure 19. Figure 19(a) focuses on the influence of reduced frequency, displaying the location where trailing edge separation initiates during the pitch up phase as a function of the incidence. Here, x/c=0 corresponds to the leading edge, while x/c=1 represents the trailing edge. It is evident from Figure 19(a) that as the reduced frequency increases, the trailing edge separation occurs over a smaller region along the aerofoil.

Figure 19(b) specifically examines the impact of blowing control. Analysing the angle of attack at 12° and 16°, it is evident that blowing has a significant effect on controlling trailing edge separation. When Cu=0.5%, the separation location shifts forward toward the leading edge, indicating that at this blowing intensity, the blowing actually promotes the occurrence of stall. In contrast, for Cu=2.6% and 5.4%, the separation location moves closer to the trailing edge, indicating effective suppression of trailing edge separation.

These findings highlight the role of reduced frequency in influencing trailing edge separation and emphasize the control capability of blowing in mitigating or exacerbating this phenomenon.

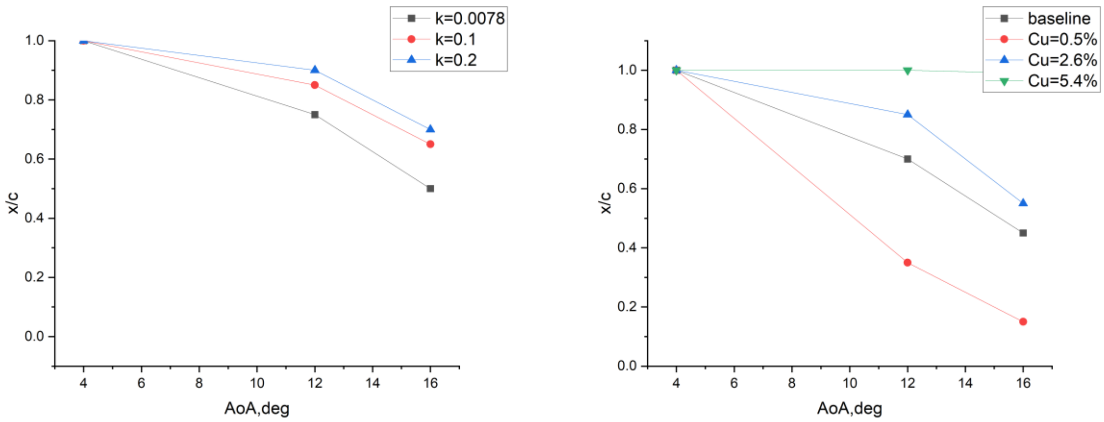

(a) (b)

Figure 19. Effect of reduced frequency(a) and blowing control momentum(b) on trailing edge separation location at different angle of attack

4. Conclusion

Leading edge blowing control, as an active method for stall control, has a significant impact on the aerodynamic performance. Our findings reveal that blowing through a slot with a high momentum coefficient leads to an increase in lift compared to the case without blowing and delays the onset of flow separation. Conversely, when employing a slot with a low momentum coefficient, the lift is reduced, and separation is induced even at lower angles of attack.

Simulations were conducted on a NACA0018 aerofoil with blowing control during pitching motion. The objective of this study was to gain insights into the impact of reduced frequency on the dynamic stall phenomenon. To analyse the flow characteristics on the suction side of the aerofoil, local lift and drag coefficients, streamline and vorticity contour plots, and skin friction coefficient distributions were utilized. These analyses aimed to provide a comprehensive understanding of the flow behaviour and its influence on the aerofoil's performance.

The aerodynamic behaviour of the pitching aerofoil was investigated for various reduced frequencies, namely k=0.0078, 0.1, and 0.2, at a Reynolds number of 250k. It was observed that as the reduced frequency increased, the lift and drag differences between pitch-up and pitch-down (hysteresis loop) generally reduced. In particular, the stall occurrence was delayed in the pitching aerofoil compared to the static case. This stall delay was prominently observed in the clean aerofoil configuration. The leading-edge fluid-blowing control method was found effective in delaying stall for the both the static and oscillating aerofoils as long as enough momentum was injected in the leading edge, in our case Cu of 2.6% and 5.4%. The leading-edge blowing was found most effective for the static condition as the rotational inertia in the fluid surrounding the oscillating aerofoil reduced the blowing effect. On the other hand, the low Cu of 0.5% hastened stall, moving the laminar separation bubble closer to the leading edge both for static and dynamic conditions. This low Cu was found to cause the boundary layer to be less energetic, pointing to the need to carefully design the leading-edge fluid-blowing control.

Acknowledgment

The first author thanks QMUL and CSC for their support to her PhD studentship. The authors also acknowledge the support of the British Council and Wohl Foundation under grant P/O4503250561

References

[1]Zhong, J., Li, J., Guo, P., & Wang, Y. ,2019, "Dynamic stall control on a vertical axis wind turbine aerofoil using leading-edge rod, " Energy, 174, pp. 246-260.

[2] Gharali K, Johnson D A., 2012, "Numerical modeling of an S809 airfoil under dynamic stall, erosion and high reduced frequencies," [J]. Applied Energy, 93, pp.45-52.

[3] Chaitanya, P., Joseph, P., Chong, T. P., Priddin, M., & Ayton, L. ,2020, "On the noise reduction mechanisms of porous aerofoil leading edges, " *Journal of Sound and Vibration*, *485*, 115574.

[4] Leishman JG. ,2002, "Challenges in modelling the unsteady aerodynamics of wind turbines, " Wind Energy 2022; 5, pp. 85–132.

[5] Leishman JG. ,2006, "Principles of Helicopter Aerodynamics, " (2nd edn), Cambridge Aerospace Series. Cambridge University Press: Cambridge.

[6] Eggleston DM, Stoddard FS. ,1987, "Wind Turbine Engineering Design". Van Nostrand Reinhold Company:New York, USA

[7] Sasson, Binyamin, and David Greenblatt. ,2011, "Effect of leading-edge slot blowing on a vertical axis wind turbine." AIAA journal 49.9, pp. 1932-1942.

[8] Müller-Vahl, H. F., Nayeri, C. N., Paschereit, C. O., & Greenblatt, D. (2016). "Dynamic stall control via adaptive blowing". *Renewable Energy*, *97*, pp. 47-64.

[9] Chen, Yang, Eldad J. Avital, and Srimanta Santra. ,2022, "Computational study of aerofoil's self-noise when subject to leading edge jet blowing flow control." 28th AIAA/CEAS Aeroacoustics 2022 Conference.
[10]Xiao, Qing, Wendi Liu, and Atilla Incecik. ,2013, "Flow control for VATT by fixed and oscillating flap." Renewable Energy 51, pp. 141-152.
[11]Greenblatt, D., Müller-Vahl, H., Lautman, R., Ben-Harav, A., & Eshel, B. ,2015, "Dielectric barrier discharge plasma flow control on a vertical axis wind turbine. " In *Active flow and combustion control* (pp. 71-86). Springer International Publishing.
[12]Greenblatt, David, and Ronen Lautman. ,2015, "Inboard/outboard plasma actuation on a vertical-axis wind turbine." Renewable Energy 83, pp. 1147-1156.
[13]Velasco, D., O. López Mejia, and S. Laín. ,2017,"Numerical simulations of active flow control with synthetic jets in a Darrieus turbine." Renewable Energy 113 , pp. 129-140.
[14]Greenblatt, D., and I. Wygnanski. ,2001, "Dynamic stall control by periodic excitation, Part 1: NACA 0015 parametric study." Journal of Aircraft 38.3,pp. 430-438.
[15] Mai, H., Dietz, G., Geißler, W., Richter, K., Bosbach, J., Richard, H., & de Groot, K. ,2008,."Dynamic stall control by leading edge vortex generators. " *Journal of the American Helicopter Society*, *53*(1), pp.26-36.
[16]Reid, E. G., and Bamber, M. J., 1928, "Preliminary Investigation on Boundary Layer Control by Means of Suction and Pressure with the U.S.A. 27 Airfoil," National Advisory Committee for Aeronautics TR-286.
[17]Knight, M., and Bamber, M. J., 1929, "Wind Tunnel Tests on Airfoil Boundary Layer Control Using a Backward Opening Slot," National Advisory Committee for Aeronautics TR-323.
[18]Poisson-Quinton, P., and Lepage, L., 1961, "Boundary Layer and Flow Control: Its Principles and Application," Survey of French Research on the Control of Boundary Layer and Circulation, edited by Lachmann, G. V., Vol. 1, Pergamon, New York, pp. 21–73.
[19]Sun, Mao, and S. R. Sheikh.,1999, "Dynamic stall suppression on an oscillating airfoil by steady and unsteady tangential blowing." Aerospace science and technology 3.6 : 355-366.
[20]Gardner, Anthony Donald, et al. "Experimental investigation of high-pressure pulsed blowing for dynamic stall control." CEAS Aeronautical Journal 5 (2014): 185-198.
[21]Müller-Vahl, Hanns F., et al. "Control of thick airfoil, deep dynamic stall using steady blowing." AIAA journal 53.2 (2015): 277-295.
[22]Müller-Vahl, Hanns Friedrich, et al. "Dynamic stall control via adaptive blowing." Renewable Energy 97 (2016): 47-64.
[23]Qijun, Z. H. A. O., M. A. Yiyang, and Z. H. A. O. Guoqing. "Parametric analyses on dynamic stall control of rotor airfoil via synthetic jet." Chinese Journal of Aeronautics 30.6 (2017): 1818-1834.

[24]Spentzos, A., et al. "CFD investigation of 2D and 3D dynamic stall." AHS International 4th Decennial Specialists' Conference on Aeromechanics. 2004.
[25]Hutomo, Go, Galih STA Bangga, and Herman Sasongko. "CFD studies of the dynamic stall characteristics on a rotating airfoil." Applied Mechanics and Materials 836 (2016): 109-114.
[26]Jain, Rohit, et al. "High-resolution computational fluid dynamics predictions for the static and dynamic stall of a finite-span OA209 wing." Journal of Fluids and Structures 78 (2018): 126-145.
[27]Zhu, Chengyong, et al. "Dynamic stall control of the wind turbine airfoil via single-row and double-row passive vortex generators." Energy 189 (2019): 116272.
[28]Ullah, Tariq, et al. "Computational evaluation of an optimum leading-edge slat deflection angle for dynamic stall control in a novel urban-scale vertical axis wind turbine for low wind speed operation." Sustainable Energy Technologies and Assessments 40 (2020): 100748.
[29]Yan, Y., Avital, E., Williams, J., & Cui, J. (2019). CFD analysis for the performance of micro-vortex generator on aerofoil and vertical axis turbine. Journal of Renewable and Sustainable Energy, 11(4).
[30]Yan, Y., Avital, E., Williams, J., & Korakianitis, T. (2019). CFD analysis for the performance of gurney flap on aerofoil and vertical axis turbine. International Journal of Mechanical Engineering and Robotics Research, 8(3), 385-392.
[31]Yan, Y., Avital, E., Williams, J., & Cui, J. (2021). Aerodynamic performance improvements of a vertical axis wind turbine by leading-edge protuberance. Journal of Wind Engineering and Industrial Aerodynamics, 211, 104535.
[32]Saleh ZJ, Avital EJ , Korakiantis T (2021), Effect of in-service burnout effect on the transonic leakage flow over cavity tip model, Proc IMechE Part A: J Power Energy, 235(8), 1847-1863
[33]Lakey S, Sangolola B. ,2007, "Aerodynamic analysis of oscillating aerofoils, including dynamic stall, using commercial CFD software. " In: 7th AIAA Aviation Technology, Integration and Operations Conference, Belfast, Northern Ireland, vol. 2, pp. 1772–85.
[34]Huang, L., Huang, P. G., LeBeau, R. P., & Hauser, T. ,2004, "Numerical study of blowing and suction control mechanism on NACA0012 airfoil. " Journal of aircraft, 41(5), pp.1005-1013.
[35]Huang, L., Huang, G., LeBeau, R., & Hauser, T. ,2007, "Optimization of aifoil flow control using a genetic algorithm with diversity control. " Journal of Aircraft, 44(4), 1337-1349.
[36]Sereez, Mohamed, and Umayr Zaffar. ,2021, "Dynamic stall on high-lift airfoil 30p30n in ground proximity." Open Journal of Fluid Dynamics 11.3 ,pp. 135-152.

[37]W. McCroskey. ,1981, "The phenomenon of dynamic stall. Technical Report, " DTIC Document